



Substrate-induced morphology and its effect on the electrical properties and stability of polycrystalline $\text{Mn}_{1.2}\text{Co}_{1.5}\text{Ni}_{0.3}\text{O}_4$ thin films

Xiangbin Wang^{1,2}, Wenwen Kong^{2,3,*} , Donglin He², Tinting Xuan^{2,3}, Jianghong Mao^{1,2,3}, Bo Gao^{2,*}, and Aimin Chang^{2,3}

¹ College of Physics Science and Technology, Xinjiang University, Urumqi, China

² CAS Key Laboratory of Functional Materials and Devices for Special Environments, Xinjiang Key Laboratory of Electronic Information Materials and Devices, Center of Materials Science and Optoelectronics Engineering, Xinjiang Technical Institute of Physics and Chemistry of CAS, Urumqi, China

³ CAS Sensor (Foshan) Technology Co., Ltd., Foshan, China

Received: 10 April 2021

Accepted: 1 August 2021

Published online:

7 August 2021

© The Author(s), under exclusive licence to Springer Science+Business Media, LLC, part of Springer Nature 2021

ABSTRACT

A series of $\text{Mn}_{1.2}\text{Co}_{1.5}\text{Ni}_{0.3}\text{O}_4$ spinel polycrystalline negative temperature coefficient (NTC) thin films on amorphous (SiO_2 and Al_2O_3) and crystalline (Si_3N_4 and AlN) substrates was prepared using the direct current sputtering technique. Electron microscopy studies reveal the morphology–substrate dependence of films grown at the optimum temperature of 200 °C, with grain size increasing in the order of $\text{Si}_3\text{N}_4 < \text{SiO}_2 < \text{AlN} < \text{Al}_2\text{O}_3$. In conjunction with XPS, both the effects of film thickness conduction and the small polaron hopping conduction mechanism on electrical properties were studied. The film thickness (205, 235, 240, and 330 nm for films grown on SiO_2 , Al_2O_3 , Si_3N_4 , and AlN substrates, respectively) showed a direct correlation to the hopping frequency of carriers in octahedron sites and affected the materials' constant, B , and temperature coefficient of resistance, α_{25} . The resistivity, ρ , of films (88.7, 202, 116.7, 279 Ω cm on SiO_2 , Al_2O_3 , Si_3N_4 , AlN substrates, respectively) was found to conform to the change rule of the change of the Mn^{3+} and Mn^{4+} ion pairs. Resistance drift values (9.39%, 6.77%, 7.37%, and 5.73% for films on SiO_2 , Al_2O_3 , Si_3N_4 , and AlN substrates, respectively) were successfully determined and suggest that films deposited on AlN substrates are the most stable for its thickness. The results presented in this paper will help guide the development and commercialization of thin film-based thermistors and development of the NTC thermistors industry.

Address correspondence to E-mail: kongww@ms.xjb.ac.cn; yunxiang0628@163.com

1 Introduction

The rapid progress of the electronic industry imposes increasing challenges as well as drives the design and development of the most common types of temperature sensors, including resistance temperature detectors (RTDs), thermocouples, and thermistors [1–4]. Among these, thermistors have attracted significant attention due to their high sensitivity for detecting small temperature changes. Most thermistors in the market are constructed in rod, disc, or bead-type structures that have high precision and the ability to withstand harsh environments. Although ceramic thin films can achieve the same functionality of their bulk form with significant savings in cost and weight [5], only a few thin-film thermistors have reached commercialization.

To date, the fabrication of high-quality thin films is largely limited to vacuum and sputtering deposition methods that employ semiconductor processing technology. The commercial exploitation of the NTCR behavior exhibited by Mn–Ni–O-based spinel-structured ceramics began in the late 1930s by the Bell Telephone Laboratories [3] and is nowadays widely used for various industrial applications for their excellent stability, accuracy, and sensitivity. Studies on the deposition and properties of Mn–Ni–O-based NTC thin films, however, were not reported until 1989 [6]. With the continued advancement in film preparation technologies and equipment conditions over the last few decades, the smoothness, density, crystallinity, and NTC character of thin films have improved dramatically. This has effectively promoted the development of NTC film research, with a significant amount of literature on the fabrication, properties, and application of Mn–Ni–O film NTC thermistors being studied [7–9].

Among the different fabrication processes, the film substrate is considered the key factor affecting the structure, performance, and stability of the deposited thin films. To date, several substrates such as SiO₂ (SiO₂ layer deposited on Si) [10, 11], Al₂O₃ [12, 13], polyimide [6, 14], glass [6, 15], MgO [16, 17], SrTiO₃ [17, 18]), AlN, and Si₃N₄ have been investigated for NTC film thermistor applications for which have been verified to be suitable for growing Mn–Co–Ni–O thin films with NTC character. Of these, amorphous SiO₂ and amorphous Al₂O₃ are most commonly used owing to their negligible effects on the crystal structure of the functional film materials. On

the other hand, SiO₂ on Si substrates with economic and integration advantages make it a favorable choice for the development of fast-response thermistor devices. The coefficient of thermal expansion (CTE) of the Al₂O₃ substrate is similar to Mn–Co–Ni–O films with a CTE of $7.6 \times 10^{-6} \text{ cm}\cdot\text{K}^{-1}$ [19, 20]. A key disadvantage, however, is that a thin oxide layer (such as amorphous SiO₂) or oxide substrate (Al₂O₃) can be easily induced to produce native defects at the interface (such as interstitials and oxygen vacancies) that may cause a deviation from stoichiometry and poor stability. Instead, Si₃N₄ and AlN substrates have been widely adopted in the field of thick-film thermistors [21]. Due to the high chemical stability, standard technological approach, and extensive fundamental importance of nitrides, such substrates do not interact with the deposited film.

In this paper, a series of Mn_{1.2}Co_{1.5}Ni_{0.3}O₄ thin films was prepared using DC magnetron on different substrates—SiO₂, Al₂O₃, Si₃N₄, and AlN—and systematically investigated. The structure, micromorphology, electrical properties, and stability of these films were investigated by exploring the stabilized mechanism of the NTC film. This work will contribute toward the development and application of NTC thin films.

2 Experimental set-up

2.1 Sample preparation

The Mn_{1.2}Co_{1.5}Ni_{0.3}O₄ thin films were prepared by two fabrication steps. Firstly, Mn_{1.2}Co_{1.5}Ni_{0.3} alloy films were sputtered onto 10 × 10 mm Si/SiO₂, Si₃N₄, Al₂O₃, and AlN substrates by a direct current (DC) magnetron sputtering system. Prior to film deposition, substrates were cleaned in acetone, absolute ethanol, and deionized water subsequently. Substrates were then placed on the sample platform in the sputtering system chamber. At a background pressure of less than $2 \times 10^{-3} \text{ Pa}$, the target was sputtered onto the substrates in an argon atmosphere (99.99%). For film deposition and film growth, the substrates' temperatures were varied (100, 150, 200, and 250 °C), while the growth pressure was fixed at 1 Pa and the sputtering power fixed at 40 W. A plasma was generated by the target for 40 min to deposit the Mn_{1.2}Co_{1.5}Ni_{0.3} films simultaneously on the four cleaned substrates. Secondly, films were

annealed at 750 °C for 30 min in air. It helps the spread of oxygen into the alloy film inside in order to realize the internal oxidation of the $\text{Mn}_{1.2}\text{Co}_{1.5}\text{Ni}_{0.3}\text{O}_4$ film.

2.2 Film characterization

The crystalline structures and preferred film orientations were determined with an X-ray diffractometer (BRUKER D8 ADVANCE, Germany) using $\text{Cu K}\alpha$ radiation. The microstructures and approximate film thicknesses were characterized using a scanning electron microscope (LEO 1430VP, Germany) and an atomic force microscope (Asylum Research MFP-3D, Britain). For electrical characterization, Cr/Au electrodes were deposited onto the prepared $\text{Mn}_{1.2}\text{Co}_{1.5}\text{Ni}_{0.3}\text{O}_4$ films [22] and the Hall effect measurements were carried out using a Hall test system (Accent HL5500 Hall System, USA). The resistance–temperature relationship in the temperature range of $-5 \sim 50$ °C was measured with a digital multimeter (KEITHLEY 3706, USA) as shown in Fig. 1. Aging tests were conducted by keeping the samples in an oven at 125 °C in air for 500 h. The aging coefficient is defined by $\Delta R/R_0 = (R_1 - R_0)/R_0$, where R_0 and R_1 are the resistances at 25 °C before and after aging, respectively.

3 Results and discussion

3.1 Crystal structure and morphology

Figure 2 reveals the grazing-incidence XRD patterns of the prepared $\text{Mn}_{1.2}\text{Co}_{1.5}\text{Ni}_{0.3}\text{O}_4$ films on SiO_2 , Al_2O_3 , Si_3N_4 , and AlN substrates. The grazing-incidence diffraction technique is particularly useful for

accurately measuring the atomic spacing of planes oriented perpendicular to the surface, which can distinguish thin films from substrate diffraction features [23]. Since the growth temperature during film deposition is responsible for the overall structure and film crystallinity, the sputtering temperature was varied between 100 and 250 °C and the resultant film structure and stability was analyzed. As shown in Fig. 2, all XRD patterns show peaks corresponding to the spinel phase PDF card No. 84-0482 and priority orientation with (311) crystal orientation. The additional diffraction peaks shown for films grown on polycrystalline AlN arise from the AlN substrate according to the PDF card No. 25-1133. Nonetheless, the main diffraction peaks at $2\theta = 30.4^\circ, 36.0^\circ, 37.4^\circ, 43.7^\circ, 54.2^\circ, 57.9^\circ,$ and 63.4° for $\text{Mn}_{1.5}\text{Co}_{1.2}\text{Ni}_{0.3}\text{O}_4$ films deposited on all four substrates agree well with the literature [24–26], confirming that the as-prepared $\text{Mn}_{1.2}\text{Co}_{1.5}\text{Ni}_{0.3}\text{O}_4$ thin films are of the single spinel-type crystal phase. With increasing growth temperature, the peak intensities show an initial increase followed by a decrease. More specifically, films sputtered at 100 °C attained the lowest peak intensities, indicative that the temperature was too low for the crystallization of $\text{Mn}_{1.2}\text{Co}_{1.5}\text{Ni}_{0.3}$ alloy films. As the growth temperature was increased from 150 °C to 200 °C, the peaks intensified which can be attributed to the enhanced diffusion velocity of atoms on the substrate and smaller enthalpy difference between the as-sputtered and the crystalline states [27, 28]. Further increases to the temperature to 250 °C resulted in a decrease in peak intensity.

The crystallinity of all the films decreases as the growth temperature increases to 250 °C as shown in the XRD pattern. The (311) peak of the films grown on SiO_2 and Al_2O_3 substrates shifts to a smaller angle,

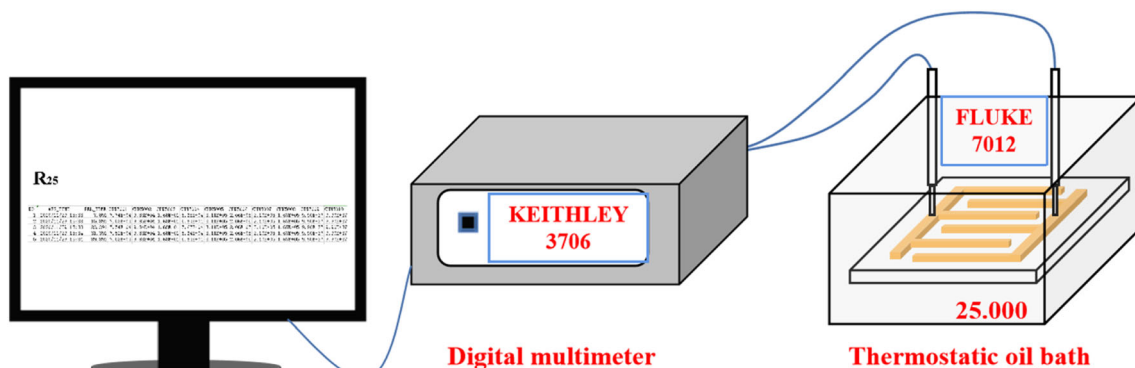
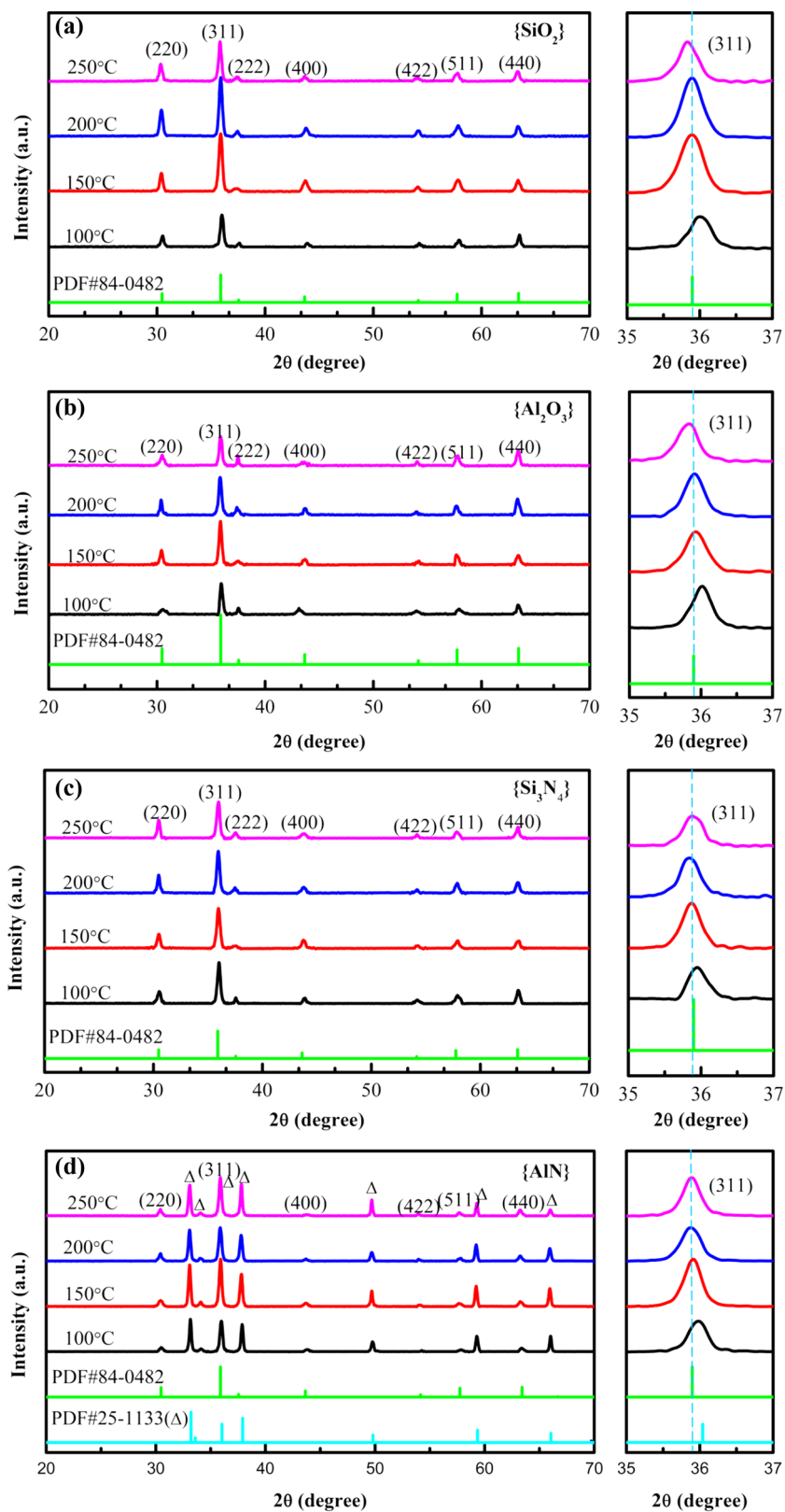


Fig. 1 The schematic diagram of the experimental test device

Fig. 2 XRD patterns of the $Mn_{1.2}Co_{1.5}Ni_{0.3}O_4$ films grown at different substrates (a- SiO_2 , b- Al_2O_3 , c- Si_3N_4 , d- AlN)



which means that the spacing between crystal faces becomes larger according to Bragg formula. It is caused by the increase of occupied ions' radius in lattice [29].

The morphology of films grown on substrates heated to 150 and 200 °C are compared to gain a thorough understanding of the relative optimal growth temperature on the four substrates. Figure 3 shows the surface and cross-sectional SEM images of the $\text{Mn}_{1.2}\text{Co}_{1.5}\text{Ni}_{0.3}\text{O}_4$ films grown on SiO_2 , Al_2O_3 , Si_3N_4 , and AlN substrates. Film thicknesses of 200 and 205 nm on SiO_2 , both 235 nm on Al_2O_3 , 235 and 240 nm on Si_3N_4 , and 325 and 330 nm on AlN at growth temperatures of 150 and 200 °C, respectively, were determined as shown in Table 1. The small differences in thickness with temperature indicate that the substrate selection forms the key influential factor.

In the deposition of thin films, the atoms arriving at the substrate mainly consist of two parts, one of atoms are absorbed to the surface by the substrate

atoms and the others escape the surface. The roughness of four substrates are tested and the results are 1.206 nm for SiO_2 , 1.214 nm for Al_2O_3 , 1.669 for Si_3N_4 , and 2.961 nm for AlN , respectively. It indicates that the roughness of AlN substrate is the largest, which leads to strong adsorption to deposited atoms on the substrate surface and weak atoms escape, resulting in thicker films grown on AlN substrate. In the process of deposition, initial aggregation (nucleation) of deposited atoms and film growth influence the grain size of the films. For majority substrates, there would produce a transition layer between substrates and films. The transition layer is the region of $\text{Mn}_{1.2}\text{Co}_{1.5}\text{Ni}_{0.3}$ amorphous alloy on the amorphous SiO_2 and Al_2O_3 substrate, while the transition layer is the region of crystal lattice distortion on monocrystal Si_3N_4 and polycrystalline AlN substrates. The different of transition layer leads to a change of nucleation and growing up and then affects the grain size and shape of the films. Although the grains are uniform and the grain boundaries are

Fig. 3 The morphology and grain size of the $\text{Mn}_{1.2}\text{Co}_{1.5}\text{Ni}_{0.3}\text{O}_4$ films sputtered at 150 °C and 200 °C (a- SiO_2 , b- Al_2O_3 , c- Si_3N_4 , d- AlN , e-grain size)

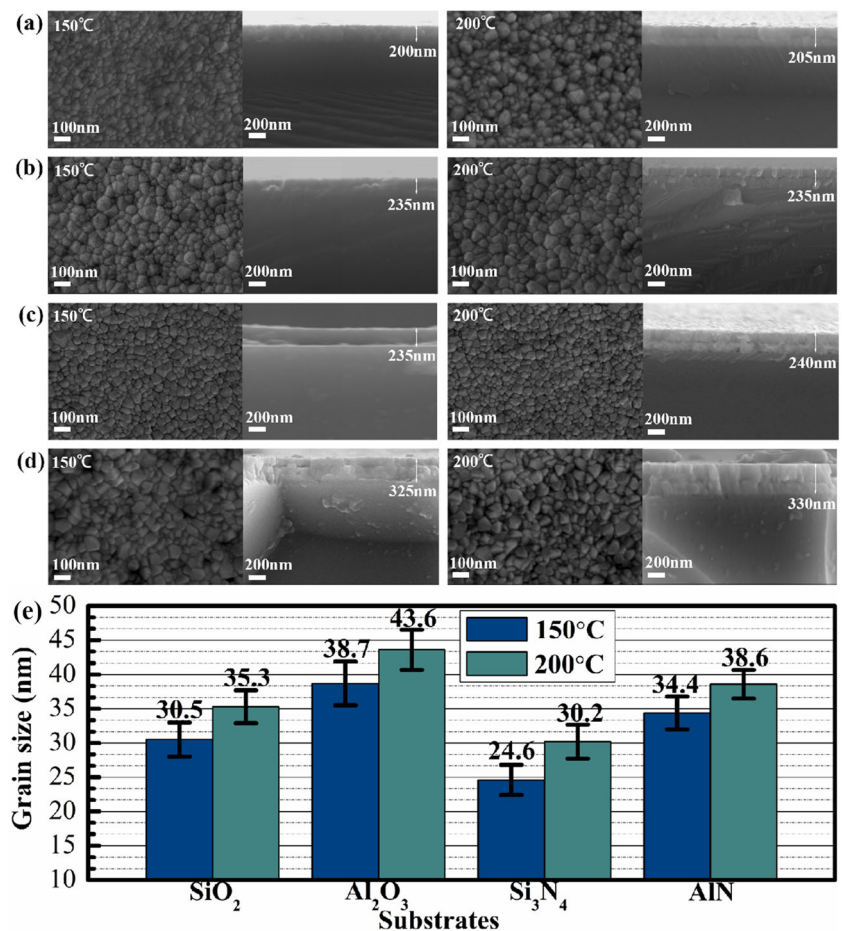


Table 1 The results of Hall test and electrical properties of films on different substrates at 200 °C

Substrates	<i>d</i> (nm)	<i>R_H</i> (cm ³ /C)	<i>ρ</i> (Ω cm)	<i>R₂₅</i> (k Ω)	<i>R₅₀</i> (k Ω)	<i>B_{25/50}</i> (K)	<i>α₂₅</i> (%/K)	<i>ΔR/R₀</i> (%)
SiO ₂	205	317	88.7	58.9	24.1	3441	− 3.9	9.39
Al ₂ O ₃	235	859	202.0	58.0	23.0	3561	− 4.0	6.77
Si ₃ N ₄	240	− 391	116.7	72.7	28.8	3565	− 4.0	7.37
AlN	330	− 592	279.0	95.8	37.4	3632	− 4.1	5.73

clear, both the grain size and roughness of films are clearly affected by the substrates. The average grain size of films was measured using Nano Measurer 1.2, the results of which are displayed in Fig. 3e and show the grain size of films increase in the order of Si₃N₄ < SiO₂ < AlN < Al₂O₃. Here, it can be seen that the grain size of films grown at 200 °C is almost 5 nm larger than those grown at 150 °C.

Figure 4 shows the AFM images of the Mn_{1.2}Co_{1.5}Ni_{0.3}O₄ films sputtered at 150 °C and 200 °C on SiO₂, Al₂O₃, Si₃N₄, and AlN substrates. It illustrates that the arithmetical average roughness (Ra) of films sputtered at 150 and 200 °C are 2.058 and 1.899 nm on SiO₂, 1.578 and 1.443 nm on Al₂O₃, 1.306 and 1.057 nm on Si₃N₄, and 2.428 and 2.047 nm on AlN, respectively. It directly indicates that the films grown at 200 °C are smoother than the 150 °C films. Hence, the films prepared at 200 °C are superior, which achieves the best smoothness.

3.2 Electrical properties

Excluding extraneous factors, making the substrate as the single variable forms the basis of this work. The electrical properties of films sputtered at 200 °C on the four substrates are studied in detail by Hall Effect measurements. Using this method, the semiconductor-type could be determined by the sign of the Hall coefficient (*R_H*), and the electrical conductivity and resistivity (*ρ*) values could also be obtained [30, 31].

Table 1 shows the results of the Hall tests and the electrical properties of films grown on different substrates at a fixed temperature of 200 °C. The Hall coefficients are 317 cm³/C on SiO₂, 859 cm³/C on Al₂O₃, − 391 cm³/C on Si₃N₄, and − 592 cm³/C on AlN. The Mn_{1.2}Co_{1.5}Ni_{0.3}O₄ polycrystalline films could be classified as either p-type or n-type semiconductors depending on the sign of the *R_H* value. The semiconductor-type of thin films grown on amorphous SiO₂ and Al₂O₃ substrates were found to be p-type, while the films grown on crystalline Si₃N₄ and polycrystalline AlN substrates were found to be

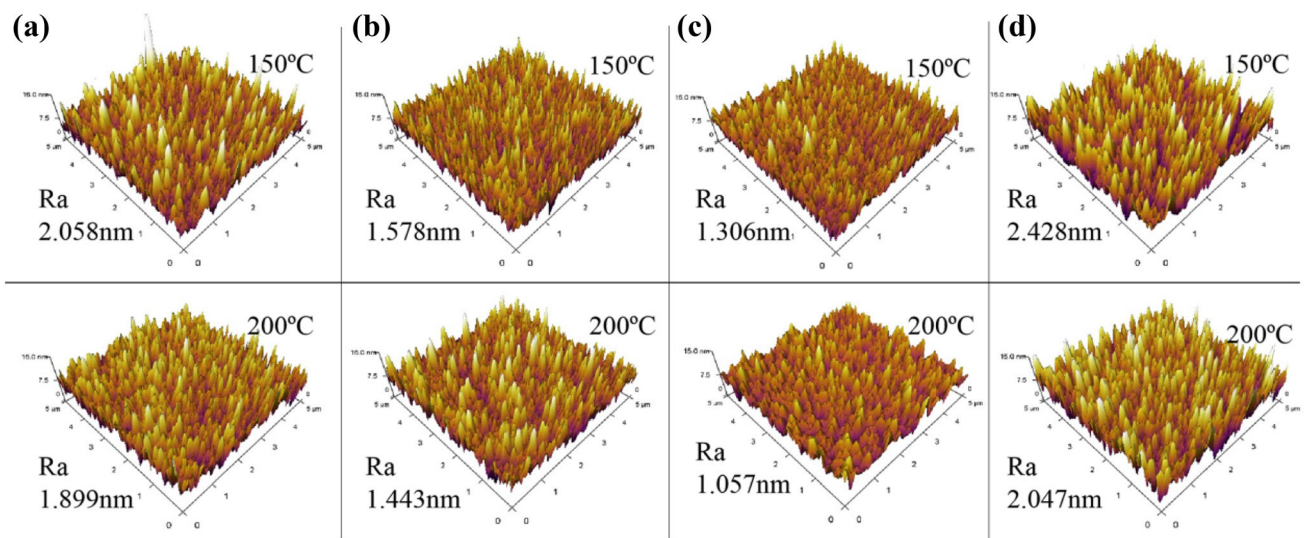


Fig. 4 The AFM images of the Mn_{1.2}Co_{1.5}Ni_{0.3}O₄ films sputtered at 150 °C and 200 °C (a-SiO₂, b-Al₂O₃, c-Si₃N₄, d-AlN)

n-type. The resistivity, ρ , for films prepared on SiO₂, Al₂O₃, Si₃N₄, and AlN substrates was found to be 88.7, 202.0, 116.7, and 279.0 Ω cm, respectively.

Generally, the electrical conduction of spinel Mn–Co–Ni–O materials is considered to occur through small polar hopping between localized Mn³⁺ and Mn⁴⁺ cations in octahedral sites. Mn2p_{3/2} XPS spectra were used to investigate the valency values and distribution of manganese ions within the films. After normalization, the peak intensities are estimated by applying a peak synthesis procedure that includes Mn²⁺ (641.3 eV), Mn³⁺ (642.5 eV), and Mn⁴⁺ (644.5 eV) as shown in Fig. 5 [32, 33]. The Mn²⁺:Mn³⁺:Mn⁴⁺ percentage ratio within each film was determined to be 26.4%: 46.2%: 27.4% on SiO₂, 45.2%: 41.5%: 13.3% on Al₂O₃, 33.4%: 43.2%: 23.4% on Si₃N₄, and 40.4%: 48.5%: 11.1% on AlN. Thus, the

percentage of Mn³⁺ and Mn⁴⁺ ion pairs is 27.4%, 13.3%, 23.4%, and 11.1% for the films grown on SiO₂, Al₂O₃, Si₃N₄, and AlN, respectively. Coupled with Table 1, the resistivity, ρ , increased with decreasing Mn³⁺ and Mn⁴⁺ ion pairs, which corresponds to the Nernst–Einstein equation [11, 34].

In addition to the film resistivity, the material constant, B , and temperature coefficient of resistance, α , play significant roles in their thermo-sensitivity for NTC applications. The resistance characteristics of the films could be described the generalized expression for small polaron hopping model as following equation: $R = CT^z \exp(T_0/T)^p$, where R is the resistance at corresponding operating temperature T , C is a constant related to temperature, T_0 is the characteristic temperature; for nearest-neighbor hopping (NNH) model, $a = p = 1$, while for variable range

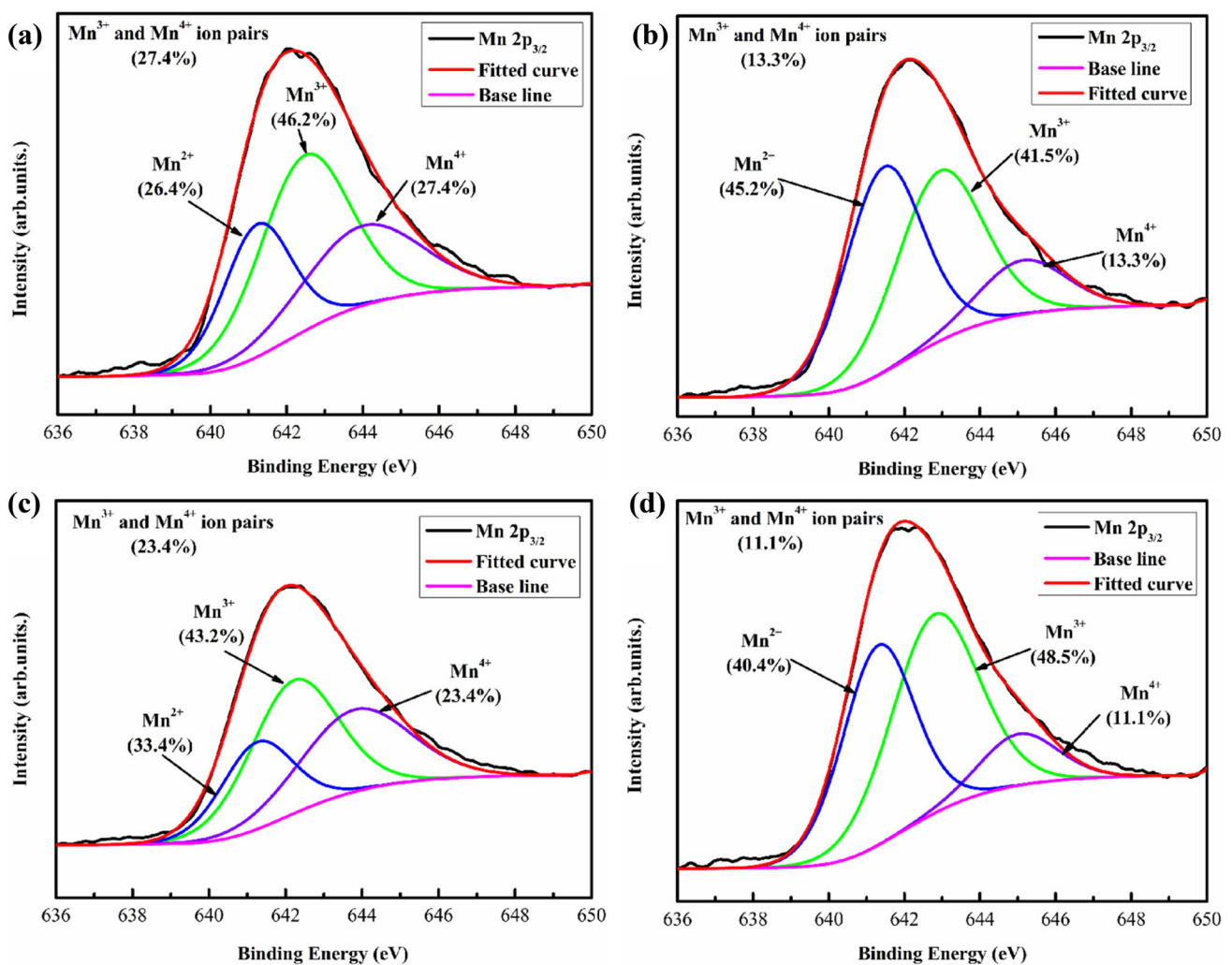


Fig. 5 XPS spectra fitting curves of the Mn_{1.2}Co_{1.5}Ni_{0.3}O₄ films grown at 200 °C before aging (a-SiO₂, b-Al₂O₃, c-Si₃N₄, d-AlN)

hopping (VRH) model, $0.25 < p = a/2 < 1$. It is possible to elucidate the electron conduction mechanism by determining p from the slope of the plots of $\ln(W)$ versus $\ln(T)$ for films as shown. The W can be described by [34, 36].

$$W = \frac{1}{T} \frac{d(\ln R)}{d(T^{-1})} \approx -p \left(\frac{T_c}{T} \right)^p \quad (1)$$

In this case, the obtained data are analyzed by linear least-squares methods. In the revision, the curve of $\ln W - \ln T$ had been supplemented as shown in Fig. 6c. The slope of the fitting line gives the value of the corresponding p . The fitting data show the p equals $1 \pm 5.29 \times 10^{-13}$, $1 \pm 1.12 \times 10^{-12}$, $1 \pm 1.06 \times 10^{-12}$, and $1 \pm 9.76 \times 10^{-13}$ for the films grown on SiO_2 , Al_2O_3 , Si_3N_4 , and AlN , respectively.

All the values of p were close to 1, which indicated that the hopping type of the films fits to NNH model.

The thermal constant, $B_{25/50}$ (/K), can be calculated using the values of R_{25} and R_{50} , with the specific formula as follows:

$$B_{50}^{25} = \frac{\ln \left(\frac{R_{25}}{R_{50}} \right)}{\left(\frac{1}{T_{25}} - \frac{1}{T_{50}} \right)} \quad (2)$$

while the temperature coefficient of resistance, α_{25} (%/K), can be calculated by the formula as follows:

$$\alpha_{25} = - \frac{B_{25/50}}{T_{25}^2} \times 100\% \quad (3)$$

By substituting R_{25} and R_{50} into formulas (2) and (3), both the $B_{25/50}$ and α_{25} can be easily obtained. The R_{25} , R_{50} , $B_{25/50}$, and α_{25} values are summarized in

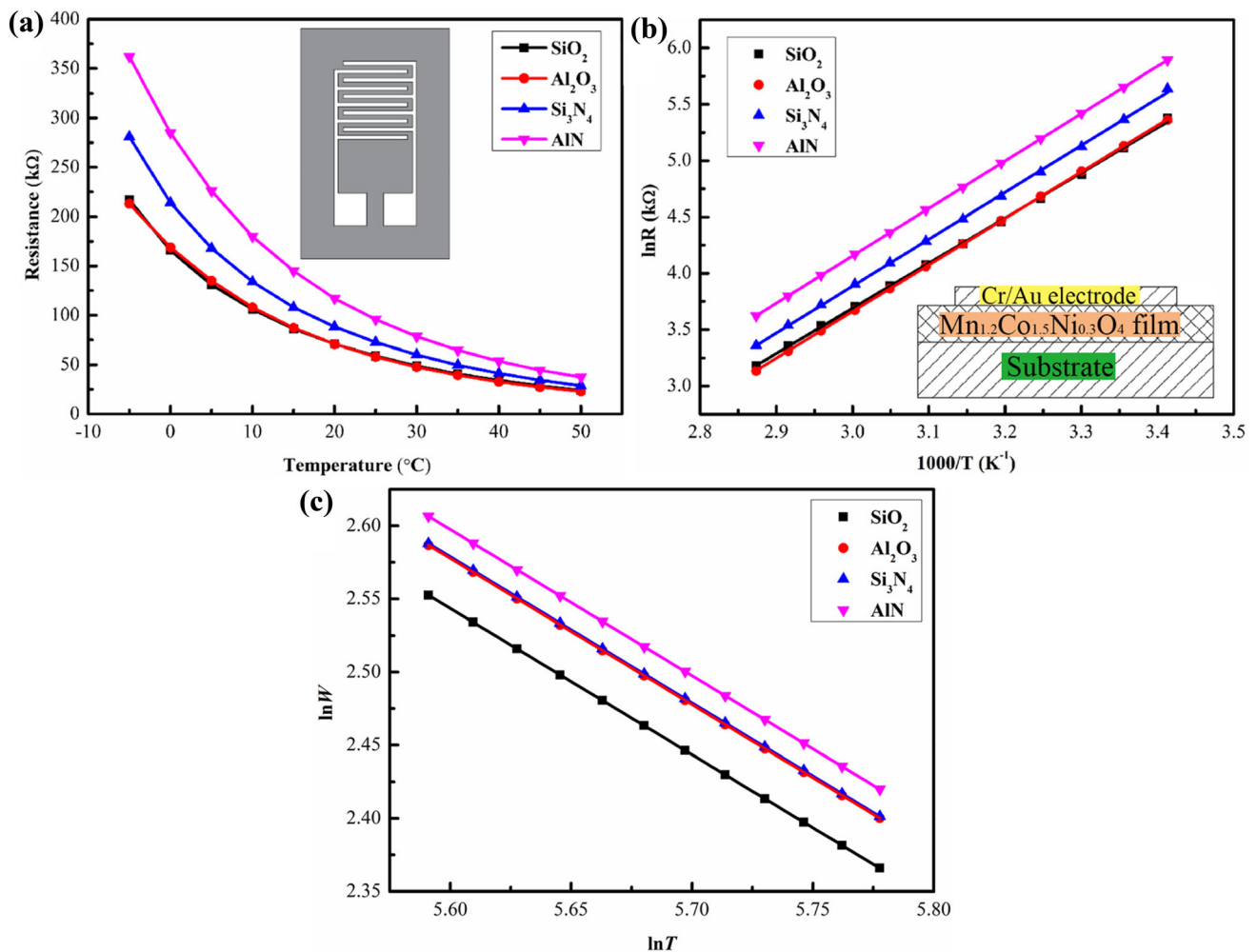


Fig. 6 a The relationship between electrical resistance and temperature. b The $\ln R$ versus $1000/T$ and c the $\ln W$ versus $\ln T$ plots for $\text{Mn}_{1.2}\text{Co}_{1.5}\text{Ni}_{0.3}\text{O}_4$ films

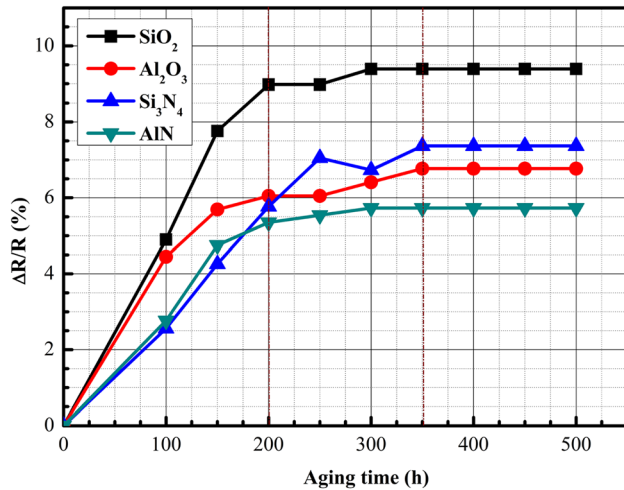


Fig. 7 The $\Delta R/R$ -aging time curves of $\text{Mn}_{1.2}\text{Co}_{1.5}\text{Ni}_{0.3}\text{O}_4$ thin films at 125 °C for 500 h

Table 1. The B values were calculated to be 3441, 3561, 3565, and 3632 K, and the α_{25} was calculated as -3.9 , -4.0 , -4.0 , and $-4.1\%/K$ for films grown on SiO_2 , Al_2O_3 , Si_3N_4 , and AlN substrates, respectively. Comparisons show that B and α_{25} values of films on different substrates exhibit only small differences but increase with thickness. This can be attributed to changes in the hopping frequency of carriers in octahedron sites which are affected by changes to thickness [11].

3.3 Stability

The aging results of $\text{Mn}_{1.2}\text{Co}_{1.5}\text{Ni}_{0.3}\text{O}_4$ films grown on SiO_2 , Al_2O_3 , Si_3N_4 , and AlN substrates after aging

at 125 °C for 500 h are shown in Fig. 7. $\Delta R/R$ -aging time curves of the four samples are similar: initially, the $\Delta R/R$ increases rapidly, after which it plateaus and keeps a stable level until 350 h. After 350 h, the resistance drift reaches 9.39%, 6.77%, 7.37%, and 5.73% for films on SiO_2 , Al_2O_3 , Si_3N_4 , and AlN substrates, respectively.

By comparing the relative resistance drift of Mn–O-based spinel films reported in the last decade (shown in Table 2), the thermal stability of the $\text{Mn}_{1.5}\text{Co}_{1.2}\text{Ni}_{0.3}\text{O}_4$ films produced here is similar to that in literature. Lin He et al. [35, 36] reported the effect of annealing temperature (650 ~ 800 °C) and thickness (400 ~ 750 nm) to resistance drift (1.7 ~ 5.2% and 5.8 ~ 11.8%) of $\text{Mn}_{1.85}\text{Co}_{0.3}\text{Ni}_{0.85}\text{O}_4$ films, which indicates the stability improved with increasing annealing temperature and decreasing thickness. Wei Ren et al. [37] reported that the resistance drift (1.02 ~ 9.53%) decreases at first and then increases with increasing annealing temperature (600 ~ 900 °C). Ruifeng Li et al. [38] reported that the resistance drift (13.27 ~ 23.56%) decreases with the increasing annealing temperature (650 ~ 900 °C). Duc Thang Le et al. [39] reported that the resistance drift (5.9 ~ 6.4%) decreases with the increase of annealing temperature (350 ~ 400 °C). By comparison, though the stability of films prepared by chemical methods appears better than those prepared by physical methods, the repeatability is worse. Additionally, the stability of films can be improved by changing substrates.

Table 2 The aging study of manganese-based thermal film

Materials	Preparation method	Substrate	Aging temperature	Aging time	$\Delta R/R_0$ (variables)
$\text{Mn}_{1.85}\text{Co}_{0.3}\text{Ni}_{0.85}\text{O}_4$ [35]	CSD	Al_2O_3	150 °C	360 h	1.7 ~ 5.2% (Annealing temperature)
$\text{Mn}_{1.85}\text{Co}_{0.3}\text{Ni}_{0.85}\text{O}_4$ [36]	CSD	Al_2O_3	150 °C	360 h	5.8 ~ 11.8% (Thickness)
$\text{Zn}_{0.4}\text{Fe}_{2.1}\text{Co}_2\text{Mn}_{1.5}\text{O}_8$ [37]	CSD	SiO_2	125 °C	500 h	1.02 ~ 9.53% (Annealing temperature)
$\text{Mn}_{1.56}\text{Co}_{0.96}\text{Ni}_{0.48}\text{O}_4$ [38]	Sputtering	SiO_2	80 °C	240 h	13.27 ~ 23.56% (Annealing temperature)
$(\text{Mn},\text{Ni},\text{Co})_3\text{O}_4$ [39]	LFD	Si	150 °C	500 h	5.9 ~ 6.4% (Annealing temperature)
$\text{Mn}_{1.2}\text{Co}_{1.5}\text{Ni}_{0.3}\text{O}_4$	Sputtering	$\text{SiO}_2/\text{Al}_2\text{O}_3/\text{Si}_3\text{N}_4/\text{AlN}$	125 °C	500 h	5.73 ~ 9.39% (Substrates)

4 Conclusion

The morphology, electrical properties, and stability of $\text{Mn}_{1.2}\text{Co}_{1.5}\text{Ni}_{0.3}\text{O}_4$ spinel films grown on different substrates were studied. Although the polycrystalline structure of the $\text{Mn}_{1.2}\text{Co}_{1.5}\text{Ni}_{0.3}\text{O}_4$ films does not differ between amorphous (SiO_2 , Al_2O_3) and crystalline (Si_3N_4 , AlN) substrates, the film grain size and thicknesses do. SEM images show that the grain size of films on different substrates grows in the order of $\text{Si}_3\text{N}_4 < \text{SiO}_2 < \text{AlN} < \text{Al}_2\text{O}_3$. Hall tests indicate that the semiconductor-type of thin films grown on amorphous SiO_2 and Al_2O_3 substrates is p-type, while the semiconductor-type of films grown on crystalline Si_3N_4 and polycrystalline AlN substrates is n-type. The thickness was found to be 205, 235, 240, and 330 nm for films grown on SiO_2 , Al_2O_3 , Si_3N_4 , and AlN substrates, respectively. This leads to changes in the hopping frequency of carriers in octahedron sites and further affects the B and α_{25} values. The ρ was determined to be 88.7, 202.0, 116.7, and 279.0 Ω cm for films on SiO_2 , Al_2O_3 , Si_3N_4 , and AlN substrates, respectively, which conforms with changes of the Mn^{3+} and Mn^{4+} ion pairs. Through aging analysis, it is found that the influence of the substrate on the resistance shift is mainly attributed to the morphology and thickness of the films.

Acknowledgements

This work was supported by the Technology Talents Project of Tianshan Youth Plan (2019Q082); the Youth Innovation Promotion Association CAS (2021433); the Xinjiang Key Laboratory Foundation (2020D04043); the Natural Science Foundation of Xinjiang, China (Grant No. 2021D01E04); and the West Light Foundation of the CAS (Grant No. 2020-XBQNXZ-001).

References

- G. Ji, A.M. Chang, J.B. Xu, H.M. Zhang, J. Hou, B. Zhang, P.J. Zhao, Low-temperature (<300 °C) growth and characterization of single-[100]-oriented Mn-Co-Ni-O thin films. *Mater. Lett.* **107**, 103–106 (2013)
- B.Y. Price, G. Hardal, Preparation and characterization of Ni-Co-Zn-Mn-O negative temperature coefficient thermistors with B_2O_3 addition. *J. Mater. Sci. Mater. Electron.* **30**, 17432–17439 (2019)
- A. Feteira, Negative temperature coefficient resistance (NTCR) ceramic thermistors: an industrial perspective. *J. Am. Ceram. Soc.* **92**, 967–983 (2009)
- W. Zhou, Y.M. Yin, J. Wu, Y.Q. Gao, Z.M. Huang, Improvements in electrical properties, low frequency noise and detection performance of a Mn-based bilayer thin film infrared detector. *Sens. Actuator A-Phys.* **283**, 196–203 (2018)
- B.W. Yang, M. He, K.H. Wen, D.P. Xiong, Y.F. Feng, S.W. Ta, Z. Yang, Comparison of morphology, electrical properties and sensitivity between bulk and thin-film $\text{Mn}_{1.5}\text{Co}_1\text{Ni}_{0.5}\text{O}_4$ thermistors. *Ceram. Int.* **46**, 27134–27142 (2020)
- S. Baliga, A.L. Jain, W. Zachofsky, Sputter deposition and characterization of Ni-Mn-O and Ni-Co-Mn-O spinels on polyimide and glass substrates. *Appl. Phys. A-Mater. Sci. Process.* **50**, 473–477 (1990)
- K. Park, Improvement in electrical stability by addition of SiO_2 in $(\text{Mn}_{1.2}\text{Ni}_{0.78}\text{Co}_{0.87-x}\text{Cu}_{0.15}\text{Si}_x)\text{O}_4$ negative temperature coefficient thermistors. *Scr. Mater.* **50**, 551–554 (2004)
- D.A. Kukuruznyak, J.G. Moyer, F.S. Ohuchi, Improved aging characteristics of NTC thermistor thin films fabricated by a hybrid sol-gel-MOD process. *J. Am. Ceram. Soc.* **89**, 189–192 (2006)
- D.F. Li, S.X. Zhao, K. Xiong, H.Q. Bao, C.W. Nan, Aging improvement in Cu-containing NTC ceramics prepared by coprecipitation method. *J. Alloys Compd.* **582**, 283–288 (2014)
- Q. Shi, W. Ren, W.W. Kong, L. Wang, C. Ma, J.B. Xu, A.M. Chang, C.Q. Jiang, Oxidation mode on charge transfer mechanism in formation of Mn-Co-Ni-O spinel films by RF sputtering. *J. Mater. Sci. Mater. Electron.* **28**, 13659–13664 (2017)
- W.W. Kong, W. Wei, B. Gao, A.M. Chang, A study on the electrical properties of Mn-Co-Ni-O thin films grown by radio frequency magnetron sputtering with different thicknesses. *Appl. Surf. Sci.* **423**, 1012–1018 (2017)
- Q. Shi, W. Ren, W.W. Kong, B. Gao, L. Wang, C. Ma, A.M. Chang, L. Bian, High B value Mn-Co-Ni spinel films on alumina substrate by RF sputtering. *J. Mater. Sci. Mater. Electron.* **28**, 9876–9881 (2017)
- W.W. Kong, J.H. Wang, J.C. Yao, A.M. Chang, Influence of oxygen atmosphere annealing on the thermal stability of $\text{Mn}_{1.2}\text{Co}_{1.5}\text{Ni}_{0.3}\text{O}_{4\pm\delta}$ ceramic films fabricated by RF magnetron sputtering. *Ceram. Int.* **44**, 1455–1460 (2018)
- W.W. Kong, W. Wei, B. Gao, A.M. Chang, $\text{Mn}_{1.56}\text{Co}_{0.96}\text{Ni}_{0.48}\text{O}_{4\pm\delta}$ flexible thin films fabricated by pulsed laser deposition for NTC applications. *Mater. Sci. Eng. B-Adv. Funct. Solid-State Mater.* **206**, 39–44 (2016)
- T. Larbi, L. Ben Said, A. Ben Daly, B. Ouni, A. Labidi, M. Amlouk, Ethanol sensing properties and photocatalytic degradation of methylene blue by Mn_3O_4 , NiMn_2O_4 and

- alloys of Ni-manganates thin films. *J. Alloys Compd.* **686**, 168–175 (2016)
16. Y.H. Xie, W.W. Kong, G. Ji, B. Gao, J.C. Yao, A.M. Chang, Growth mode and properties of Mn-Co-Ni-O NTC thermistor thin films deposited on MgO (100) substrate by laser MBE. *Mod. Phys. Lett. B* **28**, 1450235 (2014)
 17. D.J. Hagen, T.S. Tripathi, I. Terasaki, M. Karppinen, Microstructure and optical properties of ultra-thin NiO films grown by atomic layer deposition. *Semicond. Sci. Technol.* **33**, 115015 (2018)
 18. Y.W. Ma, M. Guilloux-Viry, O. Pena, C. Moure, Y(Ni, Mn)O₃ epitaxial thin films prepared by pulsed laser deposition. *Phys. Status Solidi A*. **201**, 2385–2389 (2004)
 19. C.Y. Wu, W. Zhou, Y.M. Yin, W.L. Ma, L. Jiang, Z.M. Huang, J.H. Chu, Long wavelength infrared detection based on Mn-Co-Ni-O thin films with dielectric-metal-dielectric absorptive structures. *Infrared Phys. Technol.* **102**, 102987 (2019)
 20. Y. Hou, Z.M. Huang, Y.Q. Gao, Y.J. Ge, J. Wu, J.H. Chu, Characterization of Mn_{1.56}Co_{0.96}Ni_{0.48}O₄ films for infrared detection. *Appl. Phys. Lett.* **92**, 202115 (2008)
 21. Y. Kuromitsu, T. Nagase, H. Yoshida, K. Morinaga, Development of a surface-treatment method for AlN substrates to improve adhesion with thick-film conductors. *J. Adhes. Sci. Technol.* **12**, 105–119 (1998)
 22. N. Kemik, S.V. Ushakov, M. Gu, N. Schichtel, C. Korte, N.D. Browning, Y. Takamura, A. Navrotsky, Ytria-stabilized zirconia crystallization in Al₂O₃/YSZ multilayers. *J. Mater. Res.* **6**, 939–943 (2012)
 23. D.L. Smith, *Thin-Film Deposition Principles and Practice (America Amazon)* (McGraw Hill Professional, New York, 1995), pp. 221–237
 24. B.J. Rani, R. Yuvakkumar, G. Ravi, S.I. Hong, D. Velauthapillai, R.K. Guduru, M. Thambidurai, C. Dang, W.A. Alonazi, A.M. Al-Mohaimed, Electrochemical water splitting exploration of MnCo₂O₄, NiCo₂O₄ cobaltites. *New J. Chem.* **41**, 17679–17692 (2020)
 25. B. Mandal, P. Mitra, Grain growth correlated complex impedance spectroscopy, modulus spectroscopy and carrier hopping mechanism in MnCo₂O₄: influence of sintering temperature. *Mater. Chem. Phys.* **251**, 123095 (2020)
 26. X.F. Zhou, Z.R. Jia, X.X. Zhang, B.B. Wang, X.H. Liu, B.H. Xu, L. Bi, G.L. Wu, Electromagnetic wave absorption performance of NiCo₂X₄ (X = O, S, Se, Te) spinel structures. *Chem. Eng. J.* **420**, 129907 (2021)
 27. H.X. Zhang, Z.R. Jia, B.B. Wang, X.M. Wu, T. Sun, X.H. Liu, L. Bi, G.L. Wu, Construction of remarkable electromagnetic wave absorber from heterogeneous structure of CoFe₂O₄@mesoporous hollow carbon spheres. *Chem. Eng. J.* **421**, 129960 (2021)
 28. Y.H. Lin, S.P. Chiu, J.J. Lin, Thermal fluctuation-induced tunneling conduction through metal nanowire contacts. *Nanotechnology* **19**, 365201 (2008)
 29. C.J. Ma, X.H. Chen, G.G. Lu, Y. Zhang, H. Gao, Preparation and characterization of Ni_{0.6}CoxMn_{2.4-x}O₄ (0.2 ≤ x ≤ 1.4) NTC ceramics with low resistivity and high B value. *J. Mater. Sci. Mater. Electron.* **31**, 15345–15354 (2020)
 30. J.A. Clayhold, B.M. Kerns, M.D. Schroer, D.W. Rench, G. Logvenov, A.T. Bollinger, I. Bozovic, Combinatorial measurements of Hall effect and resistivity in oxide films. *Rev. Sci. Instrum.* **79**, 033908 (2008)
 31. D.A. Neamen, *Semiconductor Physics and Devices*, 4th edn. (McGraw-Hill Education, Beijing, 2017), pp. 180–182
 32. Q. Wang, J. Zhang, W.W. Kong, Improvement of Mn_{1.56}(Co_{1-x}Al_x)_{0.96}Ni_{0.48}O₄ (0.1 ≤ x ≤ 0.4) film preparation and assessment of its structure and properties. *J. Electron. Mater.* **48**, 2077–2084 (2019)
 33. T.T. Xuan, J.Z. Yan, J.H. Wang, W.W. Kong, A.M. Chang, Characterization of Al-doped Mn-Co-Ni-O NTC thermistor films prepared by the magnetron co-sputtering approach. *J. Alloys Compd.* **831**, 154831 (2020)
 34. G. Ji, A.M. Chang, H.Y. Li, Y.H. Xie, H.M. Zhang, W.W. Kong, Epitaxial growth of Mn-Co-Ni-O thin films and thickness effects on the electrical properties. *Mater. Lett.* **130**, 127–130 (2014)
 35. L. He, Z.Y. Ling, Y.T. Huang, Y.S. Liu, Effects of annealing temperature on microstructure and electrical properties of Mn-Co-Ni-O thin films. *Mater. Lett.* **65**, 1632–1635 (2011)
 36. L. He, Z.Y. Ling, D.X. Ling, M.Y. Wu, G. Zhang, M.X. Liu, S.Q. Zhang, Role of film thickness on the microstructure and electrical properties of Mn-Co-Ni-O thin film thermistors. *Mater. Sci. Eng. B-Adv. Funct. Solid-State Mater.* **198**, 20–24 (2015)
 37. W. Ren, N.N. Zhu, L. Li, H.J. Feng, Y.G. Wang, Y.H. Yang, Z.N. Yang, S.G. Shang, Improvement of ageing issue in Zn_{0.4}Fe_{2.1}Co₂Mn_{1.5}O₈ thermistor films. *J. Eur. Ceram. Soc.* **39**, 4189–4193 (2019)
 38. R.F. Li, Q.Y. Fu, X.H. Zou, Z.P. Zheng, W. Luo, L. Yan, Mn-Co-Ni-O thin films prepared by sputtering with alloy target. *J. Adv. Ceram.* **9**, 64–71 (2020)
 39. D.T. Le, J.H. Cho, H. Ju, Annealing temperature dependent structural and electrical properties of (Mn, Ni, Co)₃O₄ thin films. *Ceram. Int.* **46**, 25536–25545 (2020)

Publisher's Note Springer Nature remains neutral with regard to jurisdictional claims in published maps and institutional affiliations.